ACES Asian Chemical Editorial Society

doi.org/10.1002/asia.202400692

CHEMISTRY AN ASIAN JOURNAL Research Article

www.chemasianj.org

Low-valent Main-group Catalysis under Ambient Conditions using a Germylene Cation**

Hemant Kumar[+],[a] Pritam Mahawar[+],[a] Purva Dua,[b] Vivek Kumar Singh,[a] Pratima Shukla,[a] Prakash Chandra Joshi,[a] Gopalan Rajaraman,[b] and Selvarajan Nagendran*[a]

Catalysis using low-valent main-group compounds is usually done under inert conditions; no example of such catalysis has been doable entirely in ambient conditions until now. This aspect is addressed in this work through an air- and water-stable germylene cation [DPMGe][(OH)B(C_6F_5)$_3$] (**2**) (DPM = dipyrromethene); it efficiently catalyzes aldehyde and ketone hydrosilylations under ambient conditions. Detailed theoretical studies reveal that compound **2**'s stability is bolstered by the interaction between the anion and germanium's frontier orbitals. However, the detachment of the anion (in the solution) alters the capability of compound **2** to render exceptional catalytic efficiency. Compound **2** was synthesized under ambient conditions by the equimolar reaction of DPMGeOH (**1**) with B(C_6F_5)$_3$.

Introduction

Many catalysts and reagents in critical processes are air-sensitive, requiring specialized techniques for handling and storage. With increasing concerns for energy usage, it is an essential facet of green chemistry to develop less energy-intensive methods for chemical production, such as catalyst systems that are air and moisture-tolerant. Recently, low-valent main-group chemistry has grown tremendously in its application in reactivity, catalysis, and materials.[1–4] As low-valent main-group compounds are air and moisture-sensitive, all these applications, including catalysis, must be pursued under inert conditions. These reactive main-group compounds have worked mainly as hydroboration, cyanosilylation, and hydrosilylation catalysts.[5–13] The first examples of these reactions done using the low-valent main-group catalysts are briefed here (Figure 1);[14–16] however, all the low-valent main-group compounds used as catalysts until now are referenced here.[17–36] Jones and coworkers used *in-situ* generated germylene **A** and stannylene **B** (Figure 1) as catalysts for the hydroboration of aldehydes and ketones.[14] Cyanosilylation of aldehydes through germylene catalyst **C** (Figure 1) was reported by the group of Nagendran.[15] Hydrosilylation of CO_2 using germylene→borane adduct **D** (Figure 1) was demonstrated by Kato and coworkers.[16]

As no example of low-valent main-group catalysis under ambient conditions has been reported until now, we report here such a possibility for the first time, eliminating the need for glove boxes, Schlenk lines, dry solvents, and special glassware. The catalyst we designed is an air and water-stable germylene cation [DPMGe][(OH)B(C_6F_5)$_3$] (**2**). It catalyzes the hydrosilylation of aldehydes and ketones in the presence of triethylsilane, offering good efficiency at room temperature.

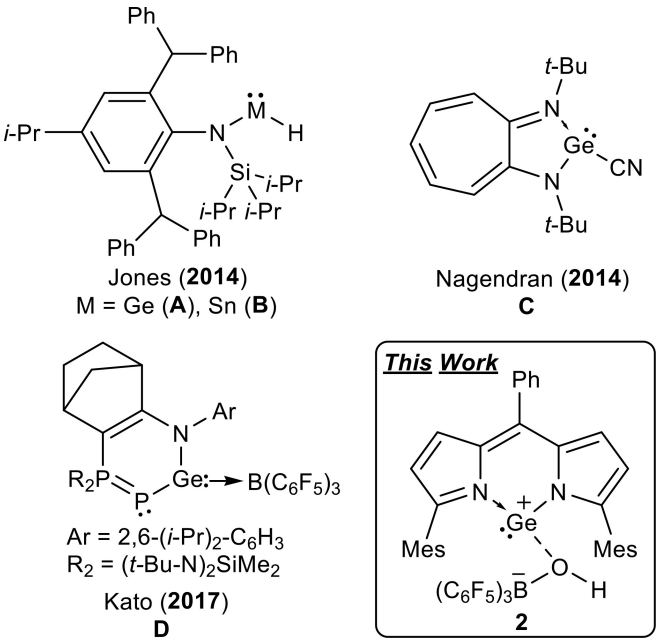

Figure 1. Examples of low-valent main group catalysts that work under inert conditions (**A**-**D**), and DPM stabilized Ge(II) cation **2** that functions under ambient conditions.

[a] *H. Kumar,[+] P. Mahawar,[+] V. K. Singh, P. Shukla, P. C. Joshi, S. Nagendran*
Department of Chemistry, Indian Institute of Technology Delhi, Hauz Khas, New Delhi 110016, India
E-mail: sisn@chemistry.iitd.ac.in

[b] *P. Dua, G. Rajaraman*
Department of Chemistry, Indian Institute of Technology Bombay, Powai, Mumbai 400076, India

[+] *Authors contributed equally.*

[**] *A previous version of this manuscript has been deposited on a preprint server (https://doi.org/10.26434/chemrxiv-2023-p4rn7).*

Supporting information for this article is available on the WWW under https://doi.org/10.1002/asia.202400692

Results and Discussion

Synthesis and Spectra

An equimolar reaction of germylene hydroxide[37] **1** with tris(pentafluorophenyl)borane in THF/toluene afforded germylene cation [DPMGe][(OH)B(C_6F_5)$_3$] (**2**) as a reddish-orange solid in 96% yield (Scheme 1). Compound **2** is soluble in toluene, tetrahydrofuran, dichloromethane, and chloroform; however, insoluble in hexane. Compound **2** provided the anticipated spectral properties during multinuclear (^{1}H, ^{13}C, ^{19}F, ^{11}B) NMR spectroscopic studies. In the ^{1}H NMR spectrum of compound **2**, the resonance signals of the mesityl methyl protons appeared as three singlets ($\delta = 1.71$, 2.12, and 2.31 ppm). A broad singlet ($\delta = 5.04$ ppm) was seen for the hydroxyl proton of the hydroxyborate anionic; in comparison to that of [PtMe(bu$_2$bpy)]$^+$[(OH)B(C_6F_5)$_3$]$^-$ (**I**, $\delta = 3.21$ ppm) that has the same hydroxyborate anionic of compound **2**, the value is downfield shifted (bu$_2$bpy = 4,4′-di-*tert*-butyl-2,2′-bipyridine).[38] The pyrrolic and mesityl groups' aromatic protons resonate as two doublets ($\delta = 6.48$ and 7.14 ppm) and singlets ($\delta = 6.87$ and 6.89 ppm), respectively. The *meso*-phenyl protons were observed as a broad singlet ($\delta = 7.63$ ppm). All the signals in the aromatic region are downfield shifted than those of compound **1**, probably due to the formal unipositive charge on the germanium atom. In the ^{11}B NMR spectrum, a broad singlet ($\delta = -1.9$ ppm) that lies in between those of B(C_6F_5)$_3$ ($\delta = -2.3$ ppm)[10] and compound **I** ($\delta = 0.1$ ppm) was observed. In the ^{19}F NMR spectrum, three signal sets ($\delta = -134.2$, -158.6, and -163.9 ppm) that are upfield shifted than those of B(C_6F_5)$_3$ ($\delta = -128$, -143, and -160 ppm) were seen. In the IR spectrum of compound **2**, an asymmetric stretching band at 3567 cm^{-1} reveals the presence of a hydroxyl group; in compound **I**, the corresponding band was observed at a higher wavenumber (3640 cm^{-1}).

Compound **2** is expected to possess a net positive charge on the germanium atom, and to affirm that this is retained even after the interaction with the hydroxide, we have performed DFT calculations (B3LYP/TZVP) using Gaussian 16 suite (see ESI).[46] The computed NPA charge on the germanium atom of compound **2** (1.277) is slightly higher than that of compound **1** (1.185). The air and water stability of compound **2** was studied through ^{1}H NMR spectroscopy. It was stable in air and water for up to 1 month and 20 days, respectively; these periods are better than compound **1** (10 and 5 days, respectively). To understand the higher stability of compound **2** compared to **1**, we have carefully analyzed their Frontier MOs, and the following points have emerged: (i) the HOMO-1 orbital corresponding to the germanium lone pair was significantly stabilized in compound **2** compared to compound **1** (62.5 kJ/mol and 20.7 kJ/mol in compounds **2** and **1**), limiting its availability for reaction with a small molecule (such as water), (ii) the empty valance p-orbitals of germanium atom are strongly delocalized (and are also in a bound state) compared to localized orbitals in compound **1** due to the π-electrons of [(OH)B(C_6F_5)$_3$]$^-$ (Figure 2), and (iii) a relatively strong interaction between germanium atom and [(OH)B(C_6F_5)$_3$]$^-$ also ensures significant steric crowding that lies along the empty p-orbitals of germanium atom blocking any possible interactions with small molecules (such as water). Thus, both steric and electronic factors provide excellent stability to compound **2** compared to compound **1**.

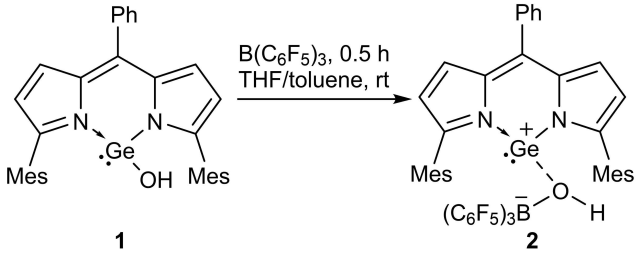

Scheme 1. Synthesis of germylene cation [DPMGe][(OH)B(C_6F_5)$_3$] (**2**).

The solid-state structure of compound **2** was established by single-crystal X-ray diffraction analysis (Figure 3). Compound **2** crystallized in the monoclinic $P2_1/n$ space group. The Ge–O bond distance (2.019 Å) in compound **2** is larger than the Ge–O bond (1.736 Å) in compound **1**; this comparison reveals the weakly coordinating nature of [(OH)B(C_6F_5)$_3$]$^-$ with the germanium center. The B–O bond length (1.529 Å) is similar to that in compound **I** (1.526 Å), where weak coordination between platinum atom and [(OH)B(C_6F_5)$_3$]$^-$ was observed.

Catalytic Utility of Compound 2

Catalytic hydrosilylation of aldehydes and ketones was carried out at ambient conditions using the fully characterized air and water stable germylene cation **2**. Benzaldehyde was chosen as the substrate for the optimization of reaction conditions. No conversion was observed when benzaldehyde was reacted with 1.2 equiv. of triethylsilane without a catalyst (entry 1, Table 1). The reaction between benzaldehyde and 1.2 equiv. of triethylsilane using 1 mol% of compound **2** as a catalyst under neat conditions for 2 h gave a conversion greater than 99% (entry 2, Table 1). Reducing the catalytic loading to 0.5 mol% gave a reduced percentage conversion of 65 (entry 3, Table 1). Further, the same reaction in solvents, such as toluene and THF, afforded less conversion to the hydrosilylated product (entries 4 and 5, Table 1). Therefore, the reaction conditions employed in entry 2 were taken as the optimized ones. Under these optimized conditions, the use of other silanes, such as Ph_3SiH and $(C_2H_5O)_2(CH_3)SiH$, in place of Et_3SiH, gave reduced percentage conversions of 81 and 37 (entries 6 and 7, Table 1). The usage of $PhSiH_3$ resulted in greater than 99% conversion (entry 8, Table 1), but the hydrosilylated product was not pure with unidentified side products. These results reveal the suitability of Et_3SiH as the hydrosilylating agent.

The substrate scope for compound **2** catalyzed hydrosilylation of aldehydes and ketones was studied by employing the optimized reaction conditions of benzaldehyde (Table 2). 2-Chlorobenzaldehyde (entry 2, Table 2) and 2-bromobenzaldehyde (entry 3, Table 2) with electron-withdrawing halo substitu-

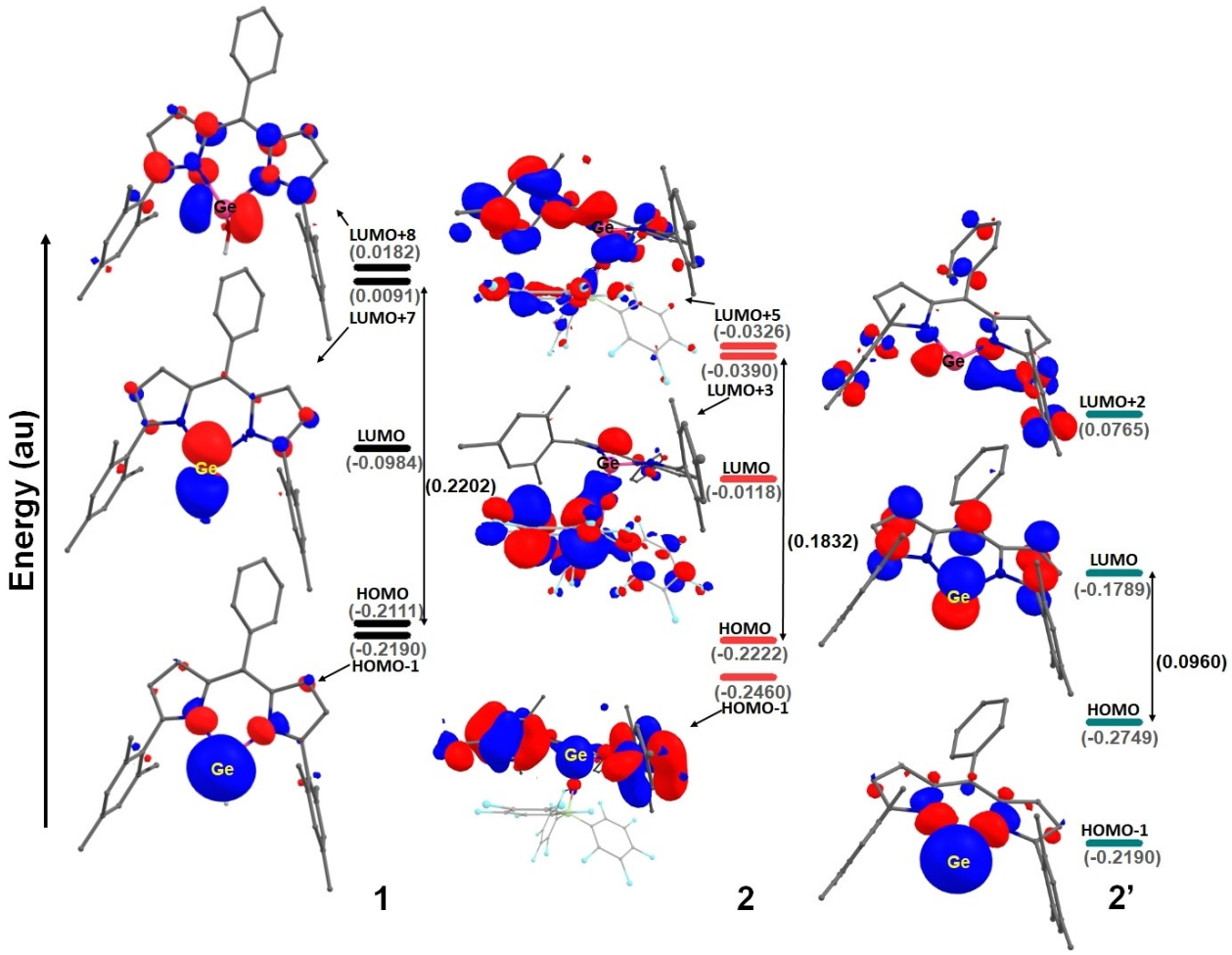

Figure 2. FMOs of compounds **1** and **2**, along with cation **2'**. Values in brackets show the energies in au.

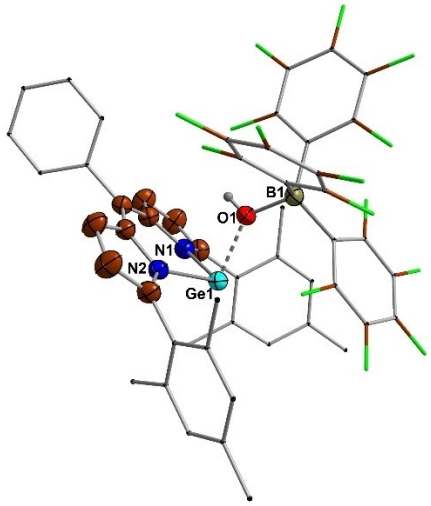

Figure 3. Molecular structure of compound **2**. All hydrogen atoms (except that of the hydroxyl group) are omitted for clarity, and thermal ellipsoids are drawn at the 30% probability level. Selected bond lengths (Å) and angles (°): Ge(1)–O(1) 2.019(2), Ge(1)–N(1) 1.963(2), Ge(1)–N(2) 1.978(2), Ge(1)–B(1) 3.290(2), O(1)–B(1) 1.529(3); O(1)–Ge(1)–N(1) 87.48(7), O(1)–Ge(1)–N(2) 91.18(7), N(1)–Ge(1)–N(2) 86.66(7), Ge(1)–O(1)–B(1) 135.6(1). (see the SI for details).

ent at *ortho*-position showed >99% conversion faster than benzaldehyde with higher TOF values of 96 and 65 h^{-1}, respectively. Considering this result, an *ortho*-disubstituted substrate, 2,6-dichlorobenzaldehyde, was tested; however, it required more time than benzaldehyde and gave a TOF of 39 h^{-1} (entry 4). Similarly, aromatic aldehydes having electron-withdrawing substituents (chloro (entry 5), bromo (entry 6), and cyano (entry 7)) at the *para*-position took more time than benzaldehyde for >99% conversion to the corresponding silylethers with a TOF of around 20 h^{-1}. However, 4-acetylbenzaldehyde, required the same time as benzaldehyde (entry 8). Aromatic aldehydes having electron-withdrawing substituents (chloro (entry 9) and nitro (entry 10)) at *meta*-position took more time than benzaldehyde and afforded a TOF close to 30 h^{-1}. 2-Methylbenzaldehyde and 4-methylbenzaldehyde with the electron-donating methyl group got hydrosilylated faster than benzaldehyde (TOF 55 and 57 h^{-1}); similarly, the hydrosilylation of heterocyclic (entry 13) and aliphatic aldehydes (entries 14 and 15) occurred quickly. The TOF (105 h^{-1}) seen with isovaleraldehyde (entry 14) is the best one in the present study. Catalyst **2** is also effective for the hydrosilylation of ketones. Acetophenone took 3 h for >99% conversion to the hydrosilylated product (TOF is 31 h^{-1}). The hydrosilylation

Table 1. Silane screening and optimization of reaction conditions for the hydrosilylation of benzaldehyde using germylene cation **2** as a catalyst.

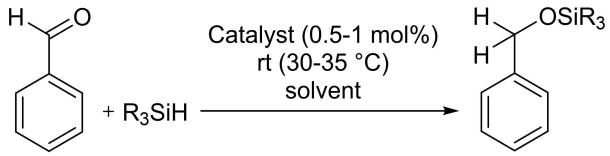

Entry	Silane	Time (h)	Solvent	Catalyst	Mol%	Conversion (%)	Yield (%)
1	Et_3SiH	2	Neat	–	–	0	0
2	Et_3SiH	2	Neat	**2**	1	>99	95
3	Et_3SiH	2	Neat	**2**	0.5	65	54
4	Et_3SiH	2	Toluene	**2**	1	31	24
5	Et_3SiH	2	THF	**2**	1	22	18
6	Ph_3SiH	2	Neat	**2**	1	81	75
7	$(EtO)_2(CH_3)SiH$	2	Neat	**2**	1	37	15
8	$PhSiH_3$	2	Neat	**2**	1	>99	39
9	Et_3SiH	2	Neat	**1**	1	0	0
10	Et_3SiH	2	Neat	DPMH	1	0	0

Conditions: Benzaldehyde (1 mmol) and silane (1.2 mmol). % Conversion was calculated by ^{1}H NMR spectroscopy; the integration of Ph*CH*O was compared with that of R*CH*$_2$(OSiR$_3$). % Yield was calculated by ^{1}H NMR spectroscopy using hexamethylbenzene as an internal standard; the integration of Ph*CH*$_2$(OSiR$_3$) was compared with that of Ph(*CH*$_3$)$_6$.

pattern of benzaldehyde derivatives is seen with acetophenone derivatives as well (which are (i) aromatic ketones with electron-donating substituents in the *para*-position have been hydrosilylated faster than the aromatic ketones containing electron-withdrawing substituents at the same position, (ii) aromatic ketones with electron-withdrawing substituents in the *ortho*-positions showed better conversion rates than aromatic ketones with electron-withdrawing substituents at the *meta*- and *para*-positions). Thus, acetophenone derivatives with an electron-withdrawing substituent at *ortho*-position (entries 17 and 18), electron-withdrawing substituent at *para*-/*meta*-position (entries 19–21), and electron-donating substituent at *ortho*-/*para*-position (entries 22–23) got hydrosilylated faster, slower, and faster than acetophenone, respectively. As anticipated, alkyl ketone, 3-methyl-2-butanone (entry 24), was hydrosilylated at a better rate than acetophenone. For diaryl ketones, benzophenone and its derivatives were studied; benzophenone gets hydrosilylated faster than acetophenone, with a TOF of 43 h^{-1}. The hydrosilylation pattern of benzaldehyde and acetophenone derivatives is partially realized with benzophenone derivatives. Thus, 2-chlorobenzophenone (entry 26) and 4-methylbenzophenone (entry 29) get hydrosilylated faster than benzophenone. However, unlike the hydrosilylation pattern of benzaldehyde and acetophenone derivatives, hydrosilylation of 3-bromobenzophenone (entry 27) and 4-bromobenzophenone (entry 28) is faster (TOF of 65 h^{-1}) than benzophenone.

The catalytic efficiency of compound **2** is compared with other main group catalysts, such as $B(C_6F_5)_3$ (**E**),[39] [Tp*AlMe][$MeB(C_6F_5)_3$] (Tp* = hydro-tris(1,3-dimethylpyrazol-1-yl)borate) (**F**),[40] [*t*-BuFcMeSi][$B(C_6F_5)_4$] (Fc = Ferrocenyl) (**G**),[41] and [LBH][$HB(C_6F_5)_3$] (**H**) (L = [{(2,4,6-$Me_3C_6H_2N$)$P(Ph_2)$}$_2$N]),[42] used for the hydrosilylation of aldehydes and ketones. The TOF values obtained using catalyst **2** for a few standard substrates (3-methyl-2-butanone, benzaldehyde, 4-methylbenzaldehyde, acetophenone, 4-methylcaetophenone, and benzophenone) are better than those obtained using catalysts (**E**, **G**, and **H**) that work at low temperatures (rt to 40 °C) (Table S1). Compound **F** is better than compound **2**; nevertheless, it operates at a much higher temperature of 75 °C (aldehydes) or 100 °C (ketones) (Table S1).

Intermolecular chemoselective hydrosilylation of aldehydes is feasible with catalyst **2**. An equimolar mixture of benzaldehyde and acetophenone, when reacted with triethylsilane using 1 mol% of compound **2** in neat condition at room temperature for 2 h, hydrosilylation of benzaldehyde only was observed. In this reaction, when acetophenone was replaced with phenylethylene, phenylacetylene, benzonitrile, or ethyl benzoate, the same result was obtained; only benzaldehyde was hydrosilylated, leaving the other compound unaffected (Scheme 2). As shown in Table 2, in the hydrosilylation of substrates, 4-cyanobenzaldeyde (entry 7), 4-acetylbenzaldehyde (entry 8),

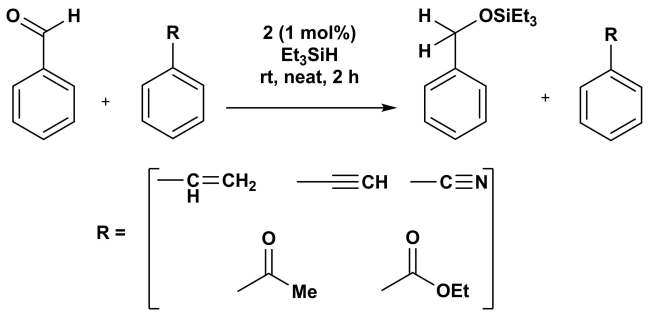

Scheme 2. Chemoselective (intermolecular) hydrosilylation of benzaldehyde.

Table 2. Substrate scope for the germylene cation **2** catalyzed hydrosilylation of aldehydes and ketones.

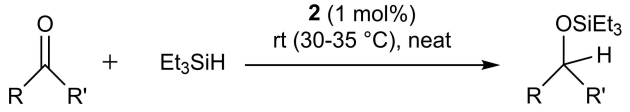

R = alkyl/aryl group, R' = H/alkyl/aryl group

Entry	R	Time (h)	% Conversion	% Yield	TOF (h^{-1})
R′ = H					
1	C_6H_5	2.0	> 99	95	48
2	2-ClC_6H_4	1.0	> 99	96	96
3	2-BrC_6H_4	1.5	> 99	97	65
4	2,6-$Cl_2C_6H_3$	2.5	> 99	97	39
5	4-ClC_6H_4	4.5	> 99	96	21
6	4-BrC_6H_4	3.75	> 99	91	24
7	4-CNC_6H_4	5.25	> 99	96	18
8*	4-$C(O)CH_3C_6H_4$	2.0	> 99	93	47
9	3-ClC_6H_4	3.0	> 99	97	32
10	3-$NO_2C_6H_4$	3.0	> 99	92	31
11	2-MeC_6H_4	1.7	> 99	94	55
12	4-MeC_6H_4	1.66	> 99	95	57
13	2-SC_4H_3	1.5	> 99	93	62
14	$CH_3(CH_2)_2$	0.91	> 99	96	105
15	$(CH_3)_2CH(CH_2)$	1.25	> 99	94	75
R′ = CH_3					
16	C_6H_5	3.0	> 99	94	31
17	2-ClC_6H_4	1.5	> 99	95	63
18	2-BrC_6H_4	1.5	> 99	98	65
19	4-ClC_6H_4	3.5	> 99	97	28
20	4-BrC_6H_4	3.25	> 99	92	28
21	3-BrC_6H_4	3.5	> 99	95	27
22	2-MeC_6H_4	1.5	> 99	98	65
23	4-MeC_6H_4	2.0	> 99	98	49
24	$(CH_3)_2CH$	1.66	> 99	92	55
R′ = C_6H_5					
25	C_6H_5	2.25	> 99	96	43
26	2-ClC_6H_4	1.0	> 99	96	96
27	3-BrC_6H_4	1.5	> 99	98	65
28	4-BrC_6H_4	1.5	> 99	97	65
29	4-MeC_6H_4	1.25	> 99	98	78

Conditions: aldehyde/ketone (1 mmol) and silane (1.2 mmol). % Conversion was calculated by ^{1}H NMR spectroscopy; for aldehydes and ketones, the integrations of RC*HO* and RC(O)R′ were compared with that of RCH_2(OSiEt_3) and R*CH*(OSiEt_3)R′ (R′ = Me, Ph). % Yield was calculated by ^{1}H NMR spectroscopy using hexamethylbenzene as an internal standard; for aldehydes and ketones, the integrations of RCH_2(OSiEt_3) and R*CH*(OSiEt_3)R′ were compared with that of Ph(CH_3)$_6$ (R′ = Me, Ph). *Only one equiv. of Et_3SiH was used.

and 3-nitrobenzaldehyde (entry 10), the cyano, keto, and nitro groups were unaffected, respectively. These data reveal the capability of catalyst **2** to hydrosilylate the aldehydic group with intramolecular chemoselectivity.

Mechanistic Study

Multinuclear NMR spectroscopy was employed to probe the mechanism of the hydrosilylation reaction catalyzed by compound **2**. The stoichiometric reaction between catalyst **2** and benzaldehyde in toluene did not lead to any product formation; it was confirmed by ^{1}H, ^{13}C, and ^{11}B NMR spectral data where the reactants remained as such after the reaction. However, in the ^{29}Si NMR spectrum (Figure S78) of the 1:1 mixture of catalyst **2** and Et_3SiH, a reasonably downfielded signal at 8.90 ppm compared to that of the free Et_3SiH (0.10 ppm) supports an adduct formation between them. In this mixture's ^{11}B NMR spectrum, a peak at −2.1 ppm is reminiscent of that of catalyst **2** (−1.9 ppm), suggesting boron's non-involvement in the catalytic cycle.

With these experimental inputs, theoretical calculations were carried out to find a plausible mechanism. The computational studies have revealed that the dissociation of [DPMGe]$^+$ and [(OH)B(C_6F_5)$_3$]$^-$ of compound **2** triggers the catalytic reaction. This cation···anion dissociation is found to be exothermic by 155.3 kJ/mol, wherein compound **2** separates to cation **2′** ([DPMGe]$^+$) and [(OH)B(C_6F_5)$_3$]$^-$. Thus, upon activation by the solvent (Et_3SiH here), the interaction between germanium and oxygen atoms is favorably broken, leading to cation **2′**. This cation subsequently serves as the catalyst to initiate the reaction (Scheme 3 and Figure 4). Considering this, the Frontier MOs of **2′** were thoroughly examined. Remarkably, the empty p-orbital of its germanium atom (LUMO) is stabilized significantly, and this is accompanied by a drastic reduction in the

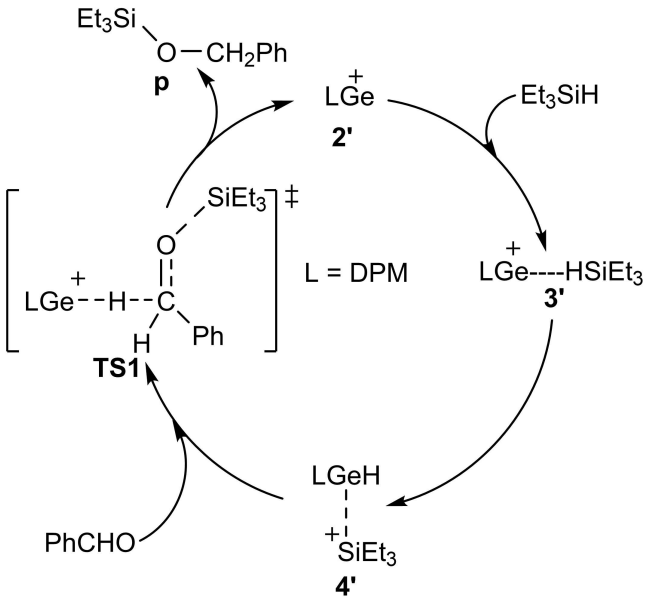

Scheme 3. Plausible catalytic cycle for the hydrosilylation of benzaldehyde by cation **2′**.

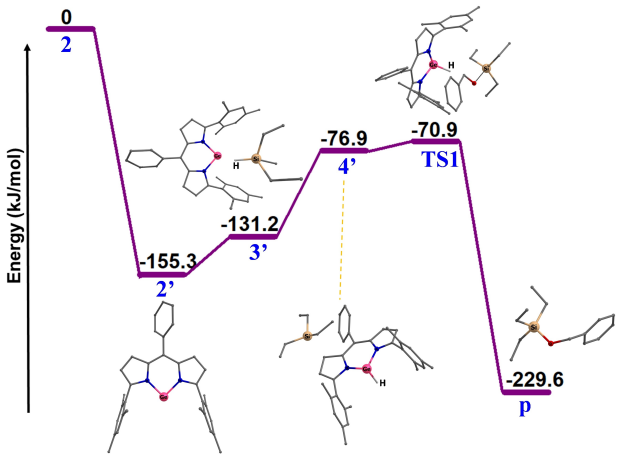

Figure 4. Energy profile diagram for the cation **2′** catalyzed hydrosilylation of benzaldehyde using Et_3SiH (Energy in kJ/mol).

HOMO-LUMO gap in comparison to compounds **1** and **2**, indicating enhanced reactivity of cation **2′** once the anionic counterpart moves away from its coordination sphere (Figure 2). The reagent Et_3SiH (acting as a solvent as well) then interacts with cation **2′**, forming cationic complex **3′** (Scheme 3, Figure 4). In **3′**, both Et_3SiH and **2′** are bound via non-covalent interaction (reactant complex); further, the formation of **3′** is slightly endothermic from **2′** (24.2 kJ/mol). However, it is an exothermic process from the original reactant (compound **2**) by 131.2 kJ/mol (Figure 4). At this stage, it is clear that the reagent is activated, and it is reflected from the Ge–H distance (2.382 Å) and Si–H bond elongation (to 1.529 Å from 1.488 Å in Et_3SiH; Figure S81). The hydride transfer to germanium occurs in the next step, leading to germylene hydride **4′**, which has a non-covalently bound triethylsilyl cation. This step is also endothermic with respect to **3′** (54.2 kJ/mol); however, compared to compound **2**, it is exothermic. As shown in Figure 2, the empty p-orbitals of the germanium atom in compound **2** are destabilized and, hence, are not susceptible to reactivity. However, in **2′**, where the anion is away, the empty 4p orbitals are getting stabilized (LUMO here), which can easily accept hydride from the Et_3SiH, leading to facile reactivity. As anticipated, in **4′**, the hydride transfer substantially reduces the charge on the germanium atom (**4′**: 0.829, **3′**: 1.259), where the length of the Ge–H bond is 1.597 Å (Scheme 3 and Figure S81). Calculations were performed to identify the transition state for hydride transfer from Et_3SiH to germylene cation in **3′**. However, our relaxed scan revealed this is a barrier-less process (Figure S82; see ESI). Once the Ge–H formation has taken place, the substrate is expected to approach **4′** in the next step, leading to the formation of the product. This process is likely to proceed via a concerted transition state **TS1** with an estimated barrier of 5.9 kJ/mol (Scheme 3). As anticipated at this transition state, both *H*···*C*H(O) (1.452 Å) and HC(*O*)···*Si* (2.150 Å) bonds are partially formed here. If compared with **4′** and **p**, it is clear that **TS1** is a reactant-like transition state, rationalizing a smaller barrier height estimated (Figures 4 and S81). The concerted bond-making and -breaking is consistent with the computed NPA charges, revealing a significant increase (decrease) in the oxygen (hydride) of the benzaldehyde (germanium) at the transition state (−0.783 in **TS1** vs. −0.502 in free benzaldehyde and −0.121 in **TS1** vs −0.215 in **4′**, Table S3; see ESI). In the last step, hydrosilylated product **p** formation occurs, which is significantly exothermic (229.6 kJ/mol). This exothermicity is expected to ease the energy demand for the subsequent catalytic cycles, rationalizing the observation of large TON and TOF values (Scheme 3 and Figure 4). Furthermore, Pier's mechanism is one of the pathways for the catalytic hydrosilylation of the carbonyl substrates (aldehydes and ketones).[39] In this pathway, the carbonyl substrate would aid in the Si–H bond cleavage after the end-on coordination of the silane to the catalyst (Figure S83, see ESI). Additional calculations were performed to rule out this possibility using benzaldehyde as the carbonyl substrate (Figure S83, see ESI); the transition state **TS′** corresponding to the Si–H bond cleavage has ~129 kJ/mol higher energy than the **2′**, and the subsequent transition state **TS″** is barrierless. However, the initially proposed mechanism for benzaldehyde hydrosilylation has a maximum energy barrier of only 84 kJ/mol from **2′** (Figure 4) and dismisses Pier's pathway being operative here. Finally, the dissociation of compound **2** into **2′** and $[HOB(C_6F_5)_3]^-$ in the presence of triethylsilane but not due to water was also examined. The Molecular Electrostatic Potential (MESP) for the catalyst **2**, water, and triethylsilane (TES) are shown in Figure S84 (see ESI). In these MESP maps, blue regions indicate positive electrostatic potential and are vulnerable to nucleophilic attack, while the red regions show negative electrostatic potential and are prone to electrophilic attack. Here, the catalyst's germanium center exhibits positive potential. Conversely, the hydrogen atom of TES and oxygen of water have a negative potential, enabling them to interact with and activate germanium. However, the steric map in Figure S84d (see ESI) shows a high buried volume of 90.7% at the germanium center, allowing only small atoms like hydrogen to access germanium and preventing access to water molecules during the reaction.

Conclusions

In conclusion, $[DPMGe][HOB(C_6F_5)_3]$ (**2**), the first example of a low-valent main-group catalyst that can operate in an ambient environment, is reported; it catalyzed the hydrosilylation of a variety of aldehydes and ketones. Detailed theoretical studies elucidate the stability of compound **2**, attributing it to the anion's interaction with the empty p-orbitals of germanium. This association destabilizes these p-orbitals to LUMO + 3 and LUMO + 5 (which otherwise should have been in LUMO). Apart from this, the association-induced steric crowding further increases the stability. Remarkably, once the anion, $[HOB(C_6F_5)_3]^-$, is detached from the cation, $[DPMGe]^+$, the empty p-orbitals of germanium are stabilized, kicking in greater reactivity and exceptional efficiency. Learning from these outcomes and encouraged by this discovery, our laboratories are pursuing designing and implementing other catalytic processes

that employ low-valent main group catalysts in ambient settings.

Author Contributions

H.K. carried out the experimental studies and drafted the manuscript. P.M. helped H.K. in the isolation of compound **2**. V.K.S. and P.S. helped H.K. during NMR studies. P.C.J. helped H.K. during ligand synthesis. P.D. and G.R. carried out the theoretical calculations. S.N. and G.R. corrected the experimental and theoretical write-ups of the manuscript, respectively.

Acknowledgements

H.K. and P.D. thank MHRD, New Delhi, India, for the Prime Minister's Research Fellowships. P.M. and P.S. thank IIT Delhi for their institute fellowships. V.K.S. and P.C.J. thank the CSIR, New Delhi, India, for research fellowships. S.N. thanks SERB, DST, New Delhi, India, for funding (CRG/2022/005756). We thank DST-FIST (SR/FST/CSII-027/2014) and the Institute of Eminence (IOE) grant from the University Grants Commission (UGC), Ministry of Human Resource and Development, India, for establishing SCXRD facilities at the Department of Chemistry, IIT Delhi. We also thank the Central Research Facility (CRF) of IIT Delhi for the NMR facility. GR would like to thank SERB for funding (SB/SJF/2019-20/12 and CRG/2022/001697).

Conflict of Interests

The authors declare no conflict of interest.

Data Availability Statement

The data that support the findings of this study are available in the supplementary material of this article.

Keywords: Germylene cation · Hydrosilylation · Main-group chemistry · Homogeneous catalysis

[1] P. P. Power, *Nature* **2010**, *463*, 171–177.
[2] C. Weetman, S. Inoue, *ChemCatChem* **2018**, *10*, 4213–4228.
[3] S. Pahar, G. Kundu, S. S. Sen, *ACS Omega* **2020**, *5*, 25477–25484.
[4] T. J. Hadlington, M. Driess, C. Jones, *Chem. Soc. Rev.* **2018**, *47*, 4176–4197.
[5] W. Wang, M. Luo, J. Li, S. A. Pullarkat, M. Ma, *Chem. Commun.* **2018**, *54*, 3042–3044.
[6] J. Li, M. Luo, X. Sheng, H. Hua, W. Yao, S. A. Pullarkat, L. Xu, M. Ma, *Org. Chem. Front.* **2018**, *5*, 3538–3547.
[7] X. Cao, J. Li, A. Zhu, F. Su, W. Yao, F. Xue, M. Ma, *Org. Chem. Front.* **2020**, *7*, 3625–3632.
[8] L. J. Morris, P. Mahawar, J. Okuda, *J. Org. Chem.* **2022**, DOI: 10.1021/acs.joc.2c02229.
[9] Z. Zhu, X. Wang, Y. Peng, H. Lei, J. C. Fettinger, E. Rivard, P. P. Power, *Angew. Chem.* **2009**, *121*, 2065–2068.
[10] Z. Li, G. Thiery, M. R. Lichtenthaler, R. Guillot, I. Krossing, V. Gandon, C. Bour, *Adv. Synth. Catal.* **2018**, *360*, 544–549.
[11] S. Yadav, S. Saha, S. S. Sen, *ChemCatChem* **2016**, *8*, 486–501.
[12] E. Fritz-Langhals, *Reactions* **2021**, *2*, 442–456.
[13] N. Sen, S. Khan, *Chem. Asian J.* **2021**, *16*, 705–719.
[14] T. J. Hadlington, M. Hermann, G. Frenking, C. Jones, *J. Am. Chem. Soc.* **2014**, *136*, 3028–3031.
[15] R. K. Siwatch, S. Nagendran, *Chem. – A Eur. J.* **2014**, *20*, 13551–13556.
[16] N. Del Rio, M. Lopez-Reyes, A. Baceiredo, N. Saffon-Merceron, D. Lutters, T. Müller, T. Kato, *Angew. Chem.* **2017**, *129*, 1385–1390.
[17] J. Schneider, C. P. Sindlinger, S. M. Freitag, H. Schubert, L. Wesemann, *Angew. Chem. Int. Ed.* **2017**, *56*, 333–337.
[18] Y. Liu, X. Liu, Y. Liu, W. Li, Y. Ding, M. Zhong, X. Ma, Z. Yang, *Inorg. Chim. Acta* **2018**, *471*, 244–248.
[19] M. Zhong, Y. Ding, D. Jin, X. Ma, Y. Liu, B. Yan, Y. Yang, J. Peng, Z. Yang, *Inorg. Chim. Acta* **2019**, *486*, 669–674.
[20] K. Nakaya, S. Takahashi, A. Ishii, K. Boonpalit, P. Surawatanawong, N. Nakata, *Dalton Trans.* **2021**, *50*, 14810–14819.
[21] S. Pahar, V. Sharma, S. Tothadi, S. S. Sen, *Dalton Trans.* **2021**, *50*, 16678–16684.
[22] M. L. Buil, J. A. Cabeza, M. A. Esteruelas, S. Izquierdo, C. J. Laglera-Gándara, A. I. Nicasio, E. Oñate, *Inorg. Chem.* **2021**, *60*, 16860–16870.
[23] V. K. Singh, P. C. Joshi, H. Kumar, R. K. Siwatch, C. K. Jha, S. Nagendran, *Dalton Trans.* **2022**, *10*, 16906–16914.
[24] R. Dasgupta, S. Das, S. Hiwase, S. K. Pati, S. Khan, *Organometallics* **2019**, *38*, 1429–1435.
[25] V. Nesterov, R. Baierl, F. Hanusch, A. E. Ferao, S. Inoue, *J. Am. Chem. Soc.* **2019**, *141*, 14576–14580.
[26] K. V. Arsenyeva, K. I. Pashanova, O. Y. Trofimova, I. V. Ershova, M. G. Chegerev, A. A. Starikova, A. V. Cherkasov, M. A. Syroeshkin, A. Y. Kozmenkova, A. V. Piskunov, *New J. Chem.* **2021**, *45*, 11758–11767.
[27] K. V. Arsenyeva, A. V. Klimashevskaya, K. I. Pashanova, O. Y. Trofimova, M. G. Chegerev, A. A. Starikova, A. V. Cherkasov, G. K. Fukin, I. A. Yakushev, A. V. Piskunov, *Appl. Organomet. Chem.* **2022**, *36*, 1–19.
[28] A. Karmakar, S. Hazra, G. M. D. M. Rúbio, M. F. C. Guedes Da Silva, A. J. L. Pombeiro, *New J. Chem.* **2018**, *42*, 17513–17523.
[29] M. M. D. Roy, S. Fujimori, M. J. Ferguson, R. McDonald, N. Tokitoh, E. Rivard, *Chem. - A Eur. J.* **2018**, *24*, 14392–14399.
[30] Y. Wu, C. Shan, Y. Sun, P. Chen, J. Ying, J. Zhu, L. Liu, Y. Zhao, *Chem. Commun.* **2016**, *52*, 13799–13802.
[31] D. Sarkar, S. Dutta, C. Weetman, E. Schubert, D. Koley, S. Inoue, *Chem. - A Eur. J.* **2021**, *27*, 13072–13078.
[32] M. K. Sharma, M. Ansari, P. Mahawar, G. Rajaraman, S. Nagendran, *Dalton Trans.* **2019**, *48*, 664–672.
[33] S. Sinhababu, D. Singh, M. K. Sharma, R. K. Siwatch, P. Mahawar, S. Nagendran, *Dalton Trans.* **2019**, *48*, 4094–4100.
[34] D. Sarkar, C. Weetman, S. Dutta, E. Schubert, C. Jandl, D. Koley, S. Inoue, *J. Am. Chem. Soc.* **2020**, *142*, 15403–15411.
[35] B. X. Leong, Y. C. Teo, C. Condamines, M. C. Yang, M. Der Su, C. W. So, *ACS Catal.* **2020**, *10*, 14824–14833.
[36] J. Lee, J. Fan, A. P. Koh, W. J. Joslyn Cheang, M. C. Yang, M. Der Su, C. W. So, *Eur. J. Inorg. Chem.* **2022**, *2022*, e202200129.
[37] P. Mahawar, M. K. Wasson, M. K. Sharma, C. K. Jha, G. Mukherjee, P. Vivekanandan, S. Nagendran, *Angew. Chem. - Int. Ed.* **2020**, *59*, 21377–21381.
[38] G. S. Hill, L. Manojlovic-Muir, K. W. Muir, R. J. Puddephatt, *Organometallics* **1997**, *16*, 525–530.
[39] a) D. J. Parks, W. E. Piers, *J. Am. Chem. Soc.* **1996**, *118*, 9440–9441; b) D. J. Parks, J. M. Blackwell, W. E. Piers, *J. Org. Chem.* **2000**, *65*, 3090–3098.
[40] J. Koller, R. G. Bergman, *Organometallics* **2012**, *31*, 2530–2533.
[41] K. Müther, M. Oestreich, *Chem. Commun.* **2011**, *47*, 334–336.
[42] S. Rawat, M. Bhandari, V. K. Porwal, S. Singh, *Inorg. Chem.* **2020**, *59*, 7195–7203.
[43] SMART, *Bruker Molecular Analysis Research Tool, Version 5.618*, Bruker AXS, Madison, WI **2000**.
[44] SAINT-NT, *Version 6.04*, Bruker AXS, WI **2001**.
[45] SHELXTL-NT, *Version 6.10*, Bruker AXS, Madison, WI **2000**.
[46] M. J. Frisch, G. W. Trucks, H. B. Schlegel, G. E. Scuseria, M. A. Robb, J. R. Cheeseman, G. Scalmani, V. Barone, G. A. Petersson, H. Nakatsuji, X. Li, M. Caricato, A. V. Marenich, J. Bloino, B. G. Janesko, R. Gomperts, B. Mennucci, H. P. Hratchian, J. V. Ortiz, A. F. Izmaylov, J. L. Sonnenberg, D. Williams-Young, F. Ding, F. Lipparini, F. Egidi, J. Goings, B. Peng, A. Petrone, T. Henderson, D. Ranasinghe, V. G. Zakrzewski, J. Gao, N. Rega, G. Zheng, W. Liang, M. Hada, M. Ehara, K. Toyota, R. Fukuda, J. Hasegawa, M. Ishida, T. Nakajima, Y. Honda, O. Kitao, H. Nakai, T. Vreven,

K. Throssell, J. A. Montgomery Jr., J. E. Peralta, F. Ogliaro, M. J. Bearpark, J. J. Heyd, E. N. Brothers, K. N. Kudin, V. N. Staroverov, T. A. Keith, R. Kobayashi, J. Normand, K. Raghavachari, A. P. Rendell, J. C. Burant, S. S. Iyengar, J. Tomasi, M. Cossi, J. M. Millam, M. Klene, C. Adamo, R. Cammi, J. W. Ochterski, R. L. Martin, K. Morokuma, O. Farkas, J. B. Foresman, D. J. Fox, Gaussian, Inc., Wallingford CT **2016**.
[47] A. D. Becke, *J. Chem. Phys.* **1997**, *107*, 8554–8560.
[48] J. Antony, S. Grimme, *Phys. Chem. Chem. Phys.* **2006**, *8*, 5287–5293.
[49] A. D. Becke, *Phys. Rev. A* **1988**, *38*, 3098–3100.
[50] A. V. Mitin, J. Baker, P. Pulay, *J. Chem. Phys.* **2003**, *118*, 7775–7783.
[51] F. Weigend, R. Ahlrichs, *Phys. Chem. Chem. Phys.* **2005**, *7*, 3297–3305.
[52] J. Tomasi, B. Mennucci, R. Cammi, *Chem. Rev.* **2005**, *105*, 2999–3093.
[53] A. P. Altshuller, L. Rosenblum, *J. Am. Chem. Soc.* **1955**, *77*, 272–274.
[54] E. D. Glendening, C. R. Landis, F. Weinhold, *J. Comput. Chem.* **2013**, *34*, 1429–1437.
[55] Deposition Number 2246362 (2) contains the supplementary crystallographic data for this paper. These data are provided free of charge by the joint Cambridge Crystallographic Data Centre and Fachinformationszentrum Karlsruhe Access Structures service. <

Manuscript received: June 14, 2024
Revised manuscript received: October 26, 2024
Accepted manuscript online: October 30, 2024
Version of record online: November 29, 2024